DOI: 10.15669/pnst.4.523

Progress in Nuclear Science and Technology
Volume 4 (2014) pp. 523-527

ARTICLE

Implementation of the exponential directional weighted S_N differencing scheme in RAPTOR-M3G for LWR radiation transport and dosimetry applications

Greg A. Fischer*

Westinghouse Electric Company LLC, 1000 Westinghouse Drive, Cranberry Township, PA 16066, USA

A high-accuracy spatial differencing scheme is implemented in RAPTOR-M3G, a Westinghouse-developed three-dimensional parallel discrete ordinates (S_N) radiation transport code. The exponential directional weighted (EDW) scheme offers enhanced accuracy and superior convergence properties compared to conventional differencing schemes at a relatively modest additional computing cost. This method enables complete convergence to typical industrial convergence thresholds on large commercial reactor problems where other differencing schemes fail. This paper explores the theoretical foundations of the EDW differencing scheme and discusses its implementation in LWR reactor problems to calculate exposure quantities of interest to the commercial reactor integrity analysis community. Comparisons to existing differencing schemes are included for several important characteristics. The computing requirements of EDW are quantified relative to the requirements of more conventional theta-weighted (TW) formulations. The convergence behavior of both methods is investigated with consideration given to spatial areas of non-convergence. Finally, the practical accuracy of both methods is assessed through comparisons of reactor dosimetry measurements to calculations from the operating fleet of commercial reactors. The EDW method and RAPTOR-M3G are demonstrated to be particularly powerful for solving the challenging three-dimensional radiation transport problems faced by today's radiation analysis community, specifically in the extended beltline region. The EDW method enables accurate characterization of the total radiation environment in large LWR models on timescales conducive to commercial applications.

Keywords: discrete ordinates S_N transport; parallel computations; reactor dosimetry; RAPTOR-M3G

1. Introduction

In the development of Pressure-Temperature (P-T) limit curves at US commercial LWRs, utilities must account for changes in fracture toughness caused by neutron embrittlement. P-T limits for normal heatup and cooldown have traditionally been based upon evaluations confined to the beltline region of the reactor vessel. However, the US Nuclear Regulatory Commission (NRC) has recently expressed concern that, due to the complex geometries of reactor vessel nozzles and penetrations, these regions may experience significantly higher stresses than regions near the beltline. In addition, the material properties in the nozzle region may be markedly inferior as compared to the beltline, or completely unknown, which may dictate more restrictive P-T curves. The NRC has suggested that future regulatory action may lower the neutron fluence evaluation threshold from 1×10^{17} n/cm^2 (E > 1.0 MeV) to 5×10^{16} n/cm^2 (E > 1.0 MeV), or implement other changes.

Such changes in regulations will likely generate increased interest in characterizing the neutron energy spectrum in the regions above and below current regions of interest. Performing neutron fluence calculations in these areas is significantly more difficult than calculating fluence for the beltline of the reactor vessel or for surveillance capsules. Importantly, neutron source distributions are more vulnerable to inaccuracies associated with nodal diffusion-based core design codes that are the current industry standard.

Obtaining confirming measurement data of the neutron spectrum near the reactor vessel nozzles can be very helpful in convincing regulators that the neutron fluence in the region is well-understood. Measurement data can be obtained by placing passive neutron sensor sets in the reactor cavity between the reactor vessel insulation and the primary concrete biological shield wall. Westinghouse has demonstrated that this data can be gathered economically and accurately, with no significant impact on plant operations [1].

For S_N calculations, an additional difficulty arises when performing calculations far outside the beltline region. Numerical oscillations in the solution begin to appear as the calculation moves farther from the neutron source. These oscillations frequently impede

*Corresponding author. Email: fischega@westinghouse.com

convergence of the model. This paper examines the oscillation phenomenon through the analysis of neutron dosimetry data from a 4-Loop PWR and implements an advanced spatial differencing scheme to address the problem.

2. Extended beltline model of a 4-Loop PWR

2.1 Description of measurements

Neutron dosimeters were installed in the reactor cavity air gap, between the reactor vessel insulation and the primary concrete biological shield wall of a 4-Loop PWR. The dosimetry set was irradiated for a single fuel cycle and then withdrawn for analysis. Each measurement location contained passive metal foil samples of the following isotopes: Cu-63, Ti-46, Fe-54, Ni-58, U-238, Np-237, and Co-59. The dosimetry samples were contained in thin-walled aluminum capsules, designed to minimize perturbations to the neutron energy spectrum.

The dosimetry capsules are attached to stainless steel gradient bead chains that run in a circular transport loop from a location immediately beneath the reactor vessel nozzles to the floor of the room underneath the reactor. A section of the circular loop is replaceable for fast and easy service of the dosimetry. In addition, the stainless steel bead chain adjacent to the dosimetry capsules can also be analyzed for its Fe-54, Ni-58, and Co-59 content. The circular loop is suspended from support bars that are connected to permanent features of the plant. **Figure 1** shows the ex-vessel neutron dosimetry system in relation to the reactor vessel and the active core.

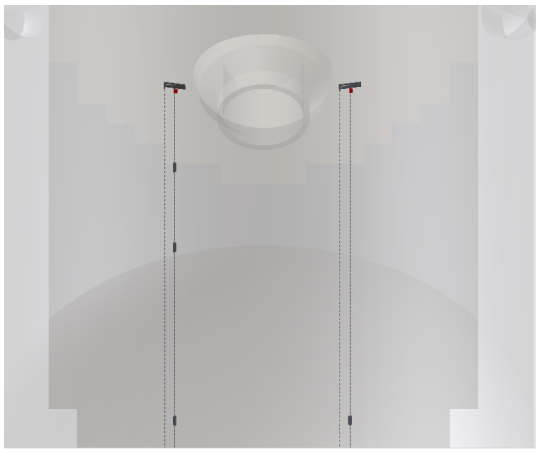

Figure 1. Ex-vessel neutron dosimetry system placement relative to a nozzle on the outside of the reactor vessel.

2.2 Computational model

The computational model used for this analysis is built upon previous work [2]. A perspective view through the fuel midplane is shown in **Figure 2**.

The 4-Loop PWR model is analyzed by RAPTOR-M3G [3]. RAPTOR-M3G is a parallel, S_N discrete ordinates radiation transport code developed by Westinghouse. It implements Theta-Weighted (TW) and Directional Theta-Weighted (DTW) solution methodologies in XYZ and RΘZ geometries.

A source particle distribution for the 4-Loop PWR model was prepared by an internal Westinghouse code. The cross section set employed for this problem was constructed from the BUGLE-96 cross section library [4]. Anisotropic scattering was treated with P_3 Legendre expansion, and the angular discretization is modeled with an S_{12} level-symmetric quadrature set. Calculated fluxes were combined with reaction cross sections from the SNLRML [5] library to produce calculated reaction rates for direct comparison with measured reaction rates.

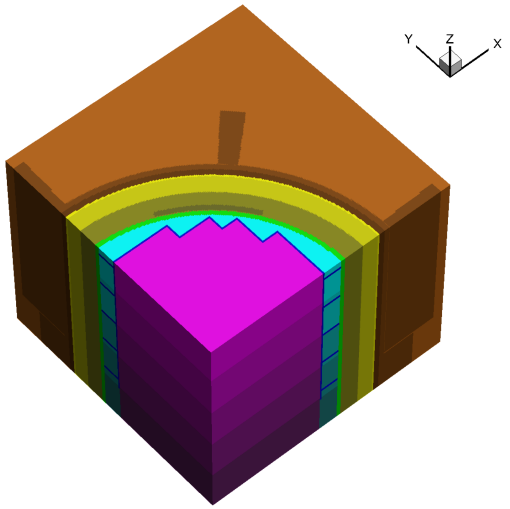

Figure 2. Plan view of the 4-Loop PWR geometry through the midplane of the active fuel. Core regions appear in purple, the reactor vessel appears yellow, and the concrete biological shield appears brown.

2.3 Convergence difficulties with existing methods

Point-wise flux convergence in RAPTOR-M3G is assessed by comparing the computed scalar (zeroth-moment) flux at iteration *i* to iteration *i-1*. Using the TW and DTW spatial differencing methods, the convergence difficulties are frequently encountered near the boundaries of the problem.

Figure 3 shows the mesh cell locations where the convergence tolerance is exceeded for DTW iteration 125 of BUGLE-96 energy group #41 (10.7 eV < E < 37.3 eV). Figure 3 shows that all regions of the problem have achieved convergence except for the areas that are near the problem boundary, mostly above the core region. Additional iterations do not substantially move the problem closer to convergence. Indeed, the specific mesh cells that fail to converge change from iteration to iteration, but the absolute number of non-converged mesh cells stays approximately constant.

The hypothesized reason for this behavior is the limited accuracy afforded by traditional TW and DTW differencing schemes. As the fixed source becomes more distant from the calculation cell, the TW and DTW schemes produce oscillations in the flux, which present the analyst with difficulty obtaining problem convergence.

To overcome these difficulties, more accurate methods are required.

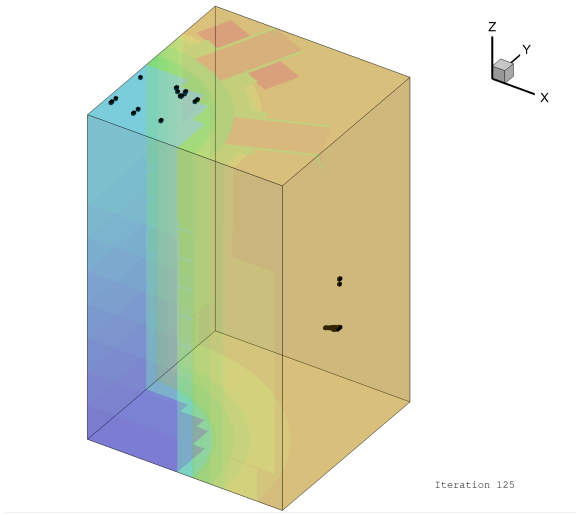

Figure 3. Radiation transport model geometry showing areas of non-convergence after 125 iterations marked in black. Colors represent different material zones in the radiation transport model.

3. Derivation of the EDW differencing scheme

The EDW scheme was proposed by Sjoden and Haghighat [6] as a means of retaining the enhanced accuracy qualities of previously-studied exponential schemes [7-8] while reducing the computational requirements to a level roughly consistent with standard weighted difference formulations.

The derivation that follows assumes nomenclature consistent with the canonical Lewis and Miller text [9]. The EDW scheme begins with the following auxiliary equation:

$$\begin{aligned}\psi_m(x,y,z) = a_0 \exp(\lambda_i P_1(x)/|\mu_m|) \\ \times \exp(\lambda_j P_1(y)/|\eta_m|) \\ \times \exp(\lambda_k P_1(z)/|\xi_m|)\end{aligned} \tag{1}$$

where $P_1(x)$, $P_1(y)$, and $P_1(z)$ are defined as first-order "shifted" Legendre functions over the mesh cell width:

$$P_1(u) = \frac{2u}{\Delta u} - 1 \tag{2}$$

and $u \in \{x,y,z\}$. The λ_i, λ_j, and λ_k terms are constants that will be defined later. The cell-average flux is calculated as:

$$\psi_A = \frac{1}{\Delta x \Delta y \Delta z}\int_0^{\Delta z}\int_0^{\Delta y}\int_0^{\Delta x}\psi_m(x,y,z)dxdydz \tag{3}$$

while the outgoing fluxes are:

$$\begin{aligned}\psi_{x\,out} &= \frac{1}{\Delta y \Delta z}\int_0^{\Delta z}\int_0^{\Delta y}\psi_m(\Delta x,y,z)dydz \\ \psi_{y\,out} &= \frac{1}{\Delta x \Delta z}\int_0^{\Delta z}\int_0^{\Delta x}\psi_m(x,\Delta y,z)dxdz \\ \psi_{z\,out} &= \frac{1}{\Delta x \Delta y}\int_0^{\Delta y}\int_0^{\Delta x}\psi_m(x,y,\Delta z)dxdy\end{aligned} \tag{4}$$

Solving Eq. (3) and Eq. (4), the outgoing angular fluxes are seen to be related to the cell center flux:

$$\begin{aligned}\psi_{x\,out} &= \psi_A \frac{2\lambda_i}{|\mu_m|}\left(1 - \exp\left(\frac{-2\lambda_i}{|\mu_m|}\right)\right)^{-1} \\ \psi_{y\,out} &= \psi_A \frac{2\lambda_j}{|\eta_m|}\left(1 - \exp\left(\frac{-2\lambda_j}{|\eta_m|}\right)\right)^{-1} \\ \psi_{z\,out} &= \psi_A \frac{2\lambda_k}{|\xi_m|}\left(1 - \exp\left(\frac{-2\lambda_k}{|\xi_m|}\right)\right)^{-1}\end{aligned} \tag{5}$$

The a_0 constant can be solved for by substituting Eq. (5) and the result of Eq. (3) into the balance equation below:

$$\begin{aligned}\frac{|\mu_m|}{\Delta x}(\psi_{x\,out} - \psi_{x\,in}) + \frac{|\eta_m|}{\Delta y}(\psi_{y\,out} - \psi_{y\,in}) + \\ \frac{|\xi_m|}{\Delta z}(\psi_{z\,out} - \psi_{z\,in}) + \sigma\psi_A = q_A\end{aligned} \tag{6}$$

In the equation above, $\psi_{x\,in}$, $\psi_{y\,in}$, and $\psi_{z\,in}$ represent the incoming angular flux on the mesh cell surface. The σ term is the total macroscopic cross-section for the energy group being calculated. The cell-averaged source, q_A, is calculated from the results of previous iterations.

Re-inserting the a_0 constant into the solution of Eq. (3) yields the following final expression for the cell center angular flux:

$$\begin{aligned}\psi_A = &\left(\exp\left(\frac{2\lambda_i}{|\mu_m|}\right) - 1\right)\left(\exp\left(\frac{2\lambda_j}{|\eta_m|}\right) - 1\right)\left(\exp\left(\frac{2\lambda_k}{|\xi_m|}\right) - 1\right) \\ &\times \frac{1}{\beta}\left(q_A + \frac{|\mu_m|}{\Delta x}\psi_{x\,in} + \frac{|\eta_m|}{\Delta y}\psi_{y\,in} + \frac{|\xi_m|}{\Delta z}\psi_{z\,in}\right)\end{aligned} \tag{7a}$$

$$\begin{aligned}\beta = &\frac{2\lambda_i}{\Delta x}\left(\exp\left(\frac{2\lambda_i}{|\mu_m|}\right)\right)\left(\exp\left(\frac{2\lambda_j}{|\eta_m|}\right) - 1\right)\left(\exp\left(\frac{2\lambda_k}{|\xi_m|}\right) - 1\right) \\ &+ \frac{2\lambda_j}{\Delta y}\left(\exp\left(\frac{2\lambda_i}{|\mu_m|}\right) - 1\right)\left(\exp\left(\frac{2\lambda_j}{|\eta_m|}\right)\right)\left(\exp\left(\frac{2\lambda_k}{|\xi_m|}\right) - 1\right) \\ &+ \frac{2\lambda_k}{\Delta z}\left(\exp\left(\frac{2\lambda_i}{|\mu_m|}\right) - 1\right)\left(\exp\left(\frac{2\lambda_j}{|\eta_m|}\right) - 1\right)\left(\exp\left(\frac{2\lambda_k}{|\xi_m|}\right)\right) \\ &+ \sigma\left(\exp\left(\frac{2\lambda_i}{|\mu_m|}\right) - 1\right)\left(\exp\left(\frac{2\lambda_j}{|\eta_m|}\right) - 1\right)\left(\exp\left(\frac{2\lambda_k}{|\xi_m|}\right) - 1\right)\end{aligned} \tag{7b}$$

The remaining unknown quantities are the exponential λ coefficients. These can be obtained by differentiating Eq. (1) in the x-, y-, and z-directions.

$$\begin{aligned} \frac{1}{\psi}\frac{\partial \psi}{\partial x} &= \frac{2\lambda_i}{\Delta x|\mu_m|} \\ \frac{1}{\psi}\frac{\partial \psi}{\partial y} &= \frac{2\lambda_j}{\Delta y|\eta_m|} \\ \frac{1}{\psi}\frac{\partial \psi}{\partial z} &= \frac{2\lambda_k}{\Delta z|\xi_m|} \end{aligned} \tag{8}$$

Assuming that the average angular flux appears at the cell center, the partial derivatives can be approximated as:

$$\left.\frac{\partial \psi}{\partial u}\right|_A \approx \frac{(\psi_{u\,out} - \psi_{u\,in})}{\Delta u} \tag{9}$$

Therefore, using the approximate relationship in Eq. (9) and rearranging Eq. (8) yields the following equation for the λ_i, λ_j, and λ_k coefficients:

$$\begin{aligned} \lambda_i &\approx \frac{(\tilde{\psi}_{x\,out} - \psi_{x\,in})|\mu_m|}{2\tilde{\psi}_A} \\ \lambda_j &\approx \frac{(\tilde{\psi}_{y\,out} - \psi_{y\,in})|\eta_m|}{2\tilde{\psi}_A} \\ \lambda_k &\approx \frac{(\tilde{\psi}_{z\,out} - \psi_{z\,in})|\xi_m|}{2\tilde{\psi}_A} \end{aligned} \tag{10}$$

The "~" symbols above the quantities in Eq. (10) indicate that suitable approximations can be obtained using an existing weighted difference formulation, such as the DTW scheme. Therefore, the EDW differencing scheme is a predictor-corrector method: DTW fluxes are used as inputs to Eq. (10), and the angular flux outputs of Eq. (5) and Eq. (7) have enhanced accuracy. Note that lambda values and exponential quantities in Eq. (5), Eq. (7), and Eq. (10) must be calculated with double precision variables and arithmetic, otherwise numerical precision problems will arise.

4. Application of the EDW method

4.1 Performance

The EDW method is more computationally intensive than a standard TW or DTW spatial differencing scheme. In addition to completing an entire DTW iteration in the predictor phase of the operation, the CPU must calculate Eq. (5), Eq. (7), and Eq. (10) during the corrector step for each computed angular flux, in each mesh cell. If the time required for a single DTW inner iteration is 1.0t seconds, testing on the problem discussed in this paper indicates that an equivalent EDW iteration requires approximately 2.2t seconds.

However, the EDW method does not need to be applied to every mesh cell. For regions that are close to the problem source, the DTW method provides adequate results at smaller computing costs. One method for applying EDW in a targeted manner is to only apply the corrector step for angular fluxes where the calculated weights in the predictor step all exceed a given threshold. A threshold of 0.96 has been found to work acceptably. This "adaptive" EDW method only requires approximately 1.1t seconds per iteration.

4.2 Convergence behavior

Table 1 compares the convergence behavior of the DTW, EDW, and Adaptive EDW methods. In the fast region, all three methods produce approximately the same behavior. However, substantial improvements are seen in the epithermal energy groups for this problem under the EDW and Adaptive EDW methods.

Using the EDW method, all energy groups achieve convergence. The decrease in the required number of iterations partially compensates for the increase in the computing time per iteration. Completion of the EDW problem required 35% more computing time than the DTW problem.

The Adaptive EDW method represents a significant improvement over the DTW method, but fails to achieve full convergence in BUGLE-96 energy group #40 due to the incomplete application of the EDW method. Nonetheless, the problem was completed in 30% less time than the DTW problem.

Table 1. Inner iterations required to achieve convergence to the threshold of ε = 1.0E-03. Entries that contain "-" indicate convergence was not achieved in 250 iterations. Note that the 250 iteration limit was removed for energy group 47.

BUGLE-96 Energy Group	$\overline{E}$ (eV)	DTW Iterations	EDW Iterations	Adaptive EDW Iterations
1	1.6E+07	33	33	33
10	2.9E+06	23	24	23
20	7.8E+05	23	23	23
30	2.9E+04	28	28	28
34	1.1E+04	228	76	77
35	5.2E+03	91	90	90
36	2.5E+03	-	86	126
37	1.0E+03	-	112	113
38	3.3E+02	-	89	108
39	1.6E+02	-	85	114
40	6.9E+01	-	103	-
41	2.4E+01	-	114	124
42	7.9E+00	-	79	78
43	3.4E+00	-	84	86
44	1.4E+00	-	64	64
45	6.5E-01	49	49	50
46	2.6E-01	56	50	51
47	5.0E-02	620	611	612

4.3 Accuracy

Comparisons of measured reaction rates to calculations appear in **Tables 2-4**, for DTW, EDW, and

Adaptive EDW, respectively. All measurements were obtained from the reactor cavity.

All methods produce similar results, with the results from the DTW and Adaptive EDW methods being nearly identical. The EDW method generally shows accuracy improvements over the DTW and Adaptive EDW methods, but the effect is minimal. The primary benefit imparted by application of EDW is the improvement in convergence behavior.

A general deterioration of the M/C comparisons can be seen when looking at dosimeters away from the core midplane. It is suspected that inaccuracies in the peripheral power distributions obtained from diffusion-based nuclear design codes are the cause of much of this deterioration.

Table 2. Ratio of Measured to Calculated (M/C) reaction rates, with calculations performed using DTW differencing.

Reaction	0° Core Midplane	45° Core Top	0° Nozzle Support
Cu-63(n,α)Co-60	1.04	0.85	0.63
Ti-46(n,p)Sc-46	1.02	0.93	0.71
Fe-54(n,p)Mn-54	1.06	0.81	0.69
Ni-58(n,p)Co-58	1.01	0.88	0.72
U-238(n,f)Cs-137	1.09	0.82	0.95
Np-237(n,f)Cs-137	1.14	0.93	1.12
Co-59(n,γ)Co-60	0.79	0.43	0.64
Co-59(n,γ)Co-60(Cd)	0.91	0.57	0.88

Table 3. Ratio of Measured to Calculated (M/C) reaction rates, with calculations performed using EDW differencing.

Reaction	0° Core Midplane	45° Core Top	0° Nozzle Support
Cu-63(n,α)Co-60	1.01	0.91	0.64
Ti-46(n,p)Sc-46	1.00	0.99	0.71
Fe-54(n,p)Mn-54	1.04	0.87	0.67
Ni-58(n,p)Co-58	0.99	0.94	0.69
U-238(n,f)Cs-137	1.08	0.88	0.91
Np-237(n,f)Cs-137	1.14	0.99	1.06
Co-59(n,γ)Co-60	0.79	0.46	0.63
Co-59(n,γ)Co-60(Cd)	0.92	0.61	0.86

Table 4. Ratio of Measured to Calculated (M/C) reaction rates, with calculations performed using EDW Adaptive differencing.

Reaction	0° Core Midplane	45° Core Top	0° Nozzle Support
Cu-63(n,α)Co-60	1.04	0.85	0.63
Ti-46(n,p)Sc-46	1.02	0.93	0.71
Fe-54(n,p)Mn-54	1.06	0.81	0.69
Ni-58(n,p)Co-58	1.01	0.88	0.72
U-238(n,f)Cs-137	1.09	0.82	0.95
Np-237(n,f)Cs-137	1.14	0.93	1.12
Co-59(n,γ)Co-60	0.79	0.44	0.64
Co-59(n,γ)Co-60(Cd)	0.92	0.58	0.88

5. Conclusion

The EDW method offers improved convergence behavior over DTW at modest additional computing cost. The Adaptive EDW method offers nearly the same convergence improvement at computing costs that are only slightly greater than DTW. Both methods have been demonstrated to meet or exceed the accuracy of DTW.

References

[1] B. Kim, C. Yoo, S. Anderson, A. Fero and C. Kim, The role of ex-vessel neutron dosimetry in reactor vessel surveillance in South Korea, *Proc. Int. Symp. on Reactor Dosimetry (ISRD-13)*, Akersloot, Netherlands, May 25-30, 2008, (2008), pp. 379-387.

[2] E. T. Hayes, *Three-Dimensional Discrete Ordinates Analysis of Ex-Vessel Neutron Dosimetry Near the Reactor Vessel Support Structure*, Pennsylvania State University, (2012).

[3] G. Longoni and S. Anderson, Reactor dosimetry applications using RAPTOR-M3G: a new parallel 3-D radiation transport code, *Proc. Int. Symp. on Reactor Dosimetry (ISRD-13)*, Akersloot, Netherlands, May 25-30, 2008, (2008), pp. 722-732.

[4] J. E. White, D. T. Ingersoll, R. Q. Wright, H. T. Hunter, C. O. Slater, N. M. Greene, R. E. MacFarlane and R. W. Roussin, *BUGLE-96, Coupled 47 Neutron and 20 Gamma-Ray Group Cross Section Library Derived from ENDF/B-VI for LWR Shielding and Pressure Vessel Dosimetry Applications*, ORNL RSICC DLC-185, Oak Ridge National Laboratory, (1996).

[5] P. J. Griffin, J. G. Kelly, T. F. Luera and J. VanDenburg, *SNLRML Recommended Dosimetry Cross-Section Compendium*, ORNL RSICC DLC-178, Oak Ridge National Laboratory, (1994).

[6] G. Sjoden and A. Haghighat, The exponential directional weighted (EDW) differencing scheme in 3-D Cartesian geometry, *Proc. Joint Int. Conf. Mathematical Methods and Supercomputing for Nuclear Applications, Saratoga Springs*, New York, October 5–9, 1997, Vol. II (1997), pp. 1267-1276.

[7] P. Barbucci and F. DiPasquantonio, Exponential supplementary equations for S_n methods: the one-dimensional case, *Nucl. Sci. Eng.*, 63 (1977), pp. 179-187.

[8] T. Wareing and R. Alcouffe, An exponential discontinuous scheme for X-Y-Z geometry transport problems, *Proc. Topl. Mtg. Radiation Protection and Shielding*, North Falmouth, Massachusetts, April 21–25, 1996, Vol. II (1996), pp. 597-605.

[9] E. E. Lewis and W. F. Miller, *Computational Methods of Neutron Transport*, American Nuclear Society, La Grange Park, Illinois, (1993). ISBN 0-89448-452-4.